We are IntechOpen, the world's leading publisher of Open Access books Built by scientists, for scientists

6,900
Open access books available

186,000
International authors and editors

200M
Downloads

154
Countries delivered to

Our authors are among the

TOP 1%
most cited scientists

12.2%
Contributors from top 500 universities

Interested in publishing with us?
Contact book.department@intechopen.com

Thin Films as a Tool for Nanoscale Studies of Cement Systems and Building Materials

Vanessa Rheinheimer and Ignasi Casanova

Additional information is available at the end of the chapter

Abstract

Many efforts have been made over the last decades to improve and develop new technologies for cement and chemical industries that can provide materials that are more durable and cost efficient, stronger and less environmentally harmful. Studies at small scale in cementitious materials usually require special sample preparation, which can damage the material and mislead the analysis. In nanoscale experiments, several techniques require samples to be extremely thin, while others need the samples to be very flat. The possibility of using thin films of clinker phases in cement research opens far-reaching opportunities for the development of this material and the materials associated to this. Testing different evaporation parameters, the deposition of films with a few tens of nanometers in thickness was achieved for all the clinker phases individually. This chapter will present the attempts for synthesizing thin films of all main clinker phases by the use of electron beam evaporation technique, as well as data on the hydration of the calcium silicate thin, flat and homogeneous samples. Changes are tracked chemically and mineralogically. This study redirects cement science to new perspectives of understanding the nanostructure of cement products. This leads to basis for developing stronger and more durable cement-based materials.

Keywords: cement, clinker phases, thin films, electron beam evaporation

1. Introduction

The Portland cement is an inorganic material, which results from burning and grounding of a raw material containing CaO, SiO_2, Al_2O_3 and small quantities of other materials. Its mixture with water results in a cement paste that sets and hardens due to a reaction called hydration. The result is a strong material that is stable even under aqueous conditions.

Cement hydration reactions take place simultaneously and in a very complex way, and understanding the behavior of such systems, with the ultimate purpose of improving durability, strength, cost and environmental impact, often requires studies at nanoscale [1].

These experiments in cementitious materials normally involve special sample preparation that can damage the material, change its properties or make it difficult to run analysis due to certain morphological characteristics of the material.

X-ray photoelectron spectroscopy (XPS) requires no special sample preparation for measurements, allowing progressive ion milling and analysis of flat surfaces to follow the progress of surface reactions [2]. In addition, in situ analyses of samples provide information not only about chemical composition but also changes in the coordination state of the elements; this has been successfully used to follow the progress of cement hydration reactions and subsequent polymerization of the materials [3–11].

Clinker is composed mainly of calcium silicates, calcium aluminate and calcium aluminoferrite. Its hydration is a very complex process, involving several phases and the formation of secondary products. Subsequently, properties of concrete are governed by processes at a molecular level with single-crystal formation. Thus, the durability and behavior of concrete during its service life strongly depend on its nanostructure.

Here, electron beam evaporation methods have been used to evaporate different clinker phases individually to synthesize thin films in an effort for producing samples suitable for nanoscale studies of cementitious materials and avoiding typical problems of sample preparation when studying these materials. This kind of sample permits elemental studies intending to design the behavior of each phase individually and the cement itself, at nanoscale, providing tools for understanding and changing the materials characteristics, looking forward to obtain better performance and durability.

Thin films techniques are widely used to produce ceramic films in the semiconductor, aerospace and optics industry, but thus far have not been applied to clinker phases. This study is an effort to develop integrated tools that allow improving the knowledge of early stage clinker phases' hydration at the molecular level and with this to better understand the behavior of these materials. With this, this work is aimed at producing clinker phase thin films suitable for hydration studies using electron beam evaporation techniques. Evaporation of each phase was repeated several times in order to optimize the most favorable experimental conditions and assess the reproducibility of the process.

2. Synthesis of clinker phases' thin films

This session describes the attempt to synthesize thin films of the four main clinker phases by means of electron beam evaporation and the outcomes. Clinker is the product from the sintering of limestone and clay during the cement manufacturing, composed mainly of four components: tricalcium silicate (C_3S), β-dicalcium silicate (C_2S), tricalcium aluminate (C_3A) and ferrite (C_4AF). Notation is the standard used in cement chemistry. Commercially available

clinker phases were used here as bulk material. All the components were 3600 cm^2/g, with free lime content below 0.5%.

Thin films were prepared with electron beam evaporation by sending a current through a tungsten filament outside the deposition zone to avoid any contamination. The filament is heated until the start of the electrons thermionic emission. Magnets focus and direct the electrons toward the bulk material that is in a constantly cooled crucible. When the electron beam hits the evaporant's surface, kinetic energy is converted into heat, releasing high energy. The evaporant boils and evaporates, condensing on the substrate and all surfaces inside the vacuum chamber. Thicknesses of the films are a function of irradiation time, estimated by an in situ quartz deposition controller.

The bulk powder phases were placed in crucibles previously cleaned with isopropyl alcohol and mounted in a vacuum chamber Univex 450B Oerlikon Leybold in a clean room. A power supply controller Telemark with a beam generating system and beam deflection unit with electromagnetic deflection for the x- and y-axis was used in the electron beam evaporator.

Sample	Crucible	Pressure (mbar)	Power (%)	I (Amp)	Voltage (Kv)	Vel_0 (Å/s)
C_3S	Graphite	$3.6–3.7 \times 10^{-4}$	3–6	0.016–0.030	7.37–7.40	0.4–1.2
C_2S	Graphite	$3.6–3.8 \times 10^{-4}$	6–10	0.022–0.050	7.30–7.42	1.1–2.5
C_3A	Graphite	3.6×10^{-4}	8–9	0.030–0.037	7.28–7.33	1–2.4
C_4AF	Boron nitride	$3.8–4.2 \times 10^{-4}$	6–11	0.018–0.056	7.26–7.32	0.1–4

Table 1. Parameters for each evaporation.

Silicon wafers with a 100 crystallographic orientation were used as deposition substrate, placed in a plate 30 cm above the crucible and held by metallic clips, and kept at ambient temperature. At a stable pressure, 4 sccm of a mix of 50% oxygen and 50% argon was inserted into the chamber to compensate the possible oxygen lost. Parameters used for each evaporation are listed in **Table 1**. The temperature in the silicon wafers was monitored and showed to be constant at room temperature during all the process; however, it is not possible to confirm the temperature achieved in the bulk sample during the evaporation.

Sample	Thickness (nm)
C_3S	280
C_2S	200
C_3A	200
C_4AF	60

Table 2. Thicknesses of the thin films.

Each sample behaved differently when bombarded by the electron beam: calcium silicate powders sublimated and did not liquefy, while during the evaporation of calcium aluminates,

the powder seemed to liquefy and higher intensities caused blasts. The resulting thin films had the thickness described in **Table 2**, measured with a profilometer.

X-ray diffraction (XRD) investigations of the bulk material were carried out in a Bruker D83 Advanced diffractometer operated at an accelerating voltage of 40 keV on a CuKα anode, irradiation intensity of 40 mA and 40 scans in steps of 0.02°/s, and results are described in the next section.

Sample	Peak position (eV) and (FWHM)					
	Ca 2p 1/2	Ca 2p 3/2	Si 2p	O 1s	Al 2p	Fe 2p
C_3S bulk	350.2 (2.5)	346.8 (2.46)	101.0 (2.83)	530.1 (2.35)		
				531.6 (2.80)		
C_3S thin film	350.2 (1.85)	346.8 (2.07)	98.2 (1.81)	529.8 (1.69)		
	351.1 (1.85)	347.5 (2.41)	100.6 (1.83)	531.2 (2.57)		
			102.4 (2.48)			
C_2S bulk	350.3 (2.41)	346.7 (2.28)	101.0 (2.68)	530.1 (2.23)		
				531.6 (2.75)		
C_2S thin film	350.4 (2.24)	346.8 (2.13)	100.8 (2.08)	530.0 (1.59)		
			101.7 (2.70)	531.3 (3.02)		
C_3A bulk	350.3 (2.43)	346.8 (2.28)		531.4 (2.15)	73.2 (2.48)	
C_3A thin film	350.6 (2.17)	347.0 (2.05)		531.5 (2.24)	–	
				533.4 (2.19)	–	
C_3A crucible	350.4 (2.03)	346.9 (2.05)		529.7 (1.5)	73.6 (1.72)	
				530.6 (2.92)	74.1 (2.25)	
C_4AF bulk	350.4 (2.25)	346.9 (2.11)		529.0 (1.95)	73.1 (2.32)	710.2 (2.60)
						711.8 (3.33)
				531.1 (2.68)		723.8 (2.29)
						725.2 (3.43)
C_4AF thin film	351.1 (2.24)	347.6 (2.44)		529.8 (1.45)	–	710.4 (2.91)
						712.6 (2.92)
				530.7 (2.82)		723.9 (2.57)
						725.8 (3.80)
C_4AF crucible	349.9 (2.51)	346.4 (2.51)		529.4 (2.13)	73.2 (1.92)	709.8 (3.70)
				531.4 (2.12)		723.0 (3.41)

Table 3. Peak position and (FWHM) for all samples.

On the other hand, due to the small diffracting volumes, which result in low intensities compared to the substrate and background, mineralogical phases on thin films are difficult to be identified. GIXRD allows increasing the intensity of the signal produced from the film by increasing the path length of the incident X-ray beam through it, so that conventional phase identification analysis can be run [12–14]. GIXRD experiments were performed using a Bragg-Brentano Siemens D-500 X-ray diffractometer at 45 kV accelerating voltage, on a CuKα anode, with 40 mA irradiation intensity and 0.05°/s steps, with an incident angle of w = 0.4°. No monochromator was used to increase the signal. Different detector apertures were used for each sample, depending on their size.

Chemical composition of a material's surface was assessed by XPS, which works by irradiating the sample with a X-rays beam and measuring both the kinetic energy and the number of electrons escaping from its surface.

Chemical composition of the thin films was verified using a SPECS™ X-ray photoelectron spectroscopy system equipped with an XR50 Al anode source operating at 150 W and a Phoibos MCD-9 detector. Spectra were recorded with pass energy of 25 eV at 0.1 eV steps at a pressure below 10^{-9} mbar.

For analysis of the bulk material, powder was pressed into pellets and fixed onto holders with a copper tape, same fixing as the silicon wafers with the thin films. For each sample, general scan was repeated three times, and specific high-resolution scans were carried out for elements of interest, such as calcium, silicon, carbon, oxygen, iron and aluminum. Data were extracted from the spectra via peak fitting using CasaXPS™ software. Shirley background was assumed in all cases. The adventitious carbon peak at 284.8 eV was used for correction of the charging effects. Three scans with a passing energy of 5 eV were carried out for the acquisition of each pattern.

XPS binding energies (BEs) and full width half maximum (FWHM) peak parameters are shown in **Table 3**.

2.1. Calcium silicates

The similarity between the GIXRD patterns of the bulk material and the XRD of the thin film (**Figure 1a**) strongly suggests that the evaporated and recondensed material keeps the mineralogical composition of the original bulk material. Even with the relatively faint signal observed due to the thickness of the film and the high noise level, the presence of the most intense peaks of C_3S (at 32.07°, 34.29° and 32.33°) is clearly noticed as a broad peak in the pattern. This broadening in the peaks has been observed in several other researches when working with thin films, specially using Bragg-Brentano configuration [15–17]. This is likely due to the thin film's poor crystallinity.

Similarly to C_3S, the C_2S samples show a strong match between the diffraction patterns of bulk material and thin film (**Figure 1b**). The same low signal and high noise are observed, but the presence of the most intense peaks of C_2S (at 31.98°, 32.38° and 40.55°) is coincident with the broad peak in the thin film spectrum, suggesting that the evaporated material keeps the bulk mineralogical composition. Even the broad peak at low degrees is observed in both spectra,

which can be either due to the presence of amorphous material or an artifact of the technique due to the small size of the sample.
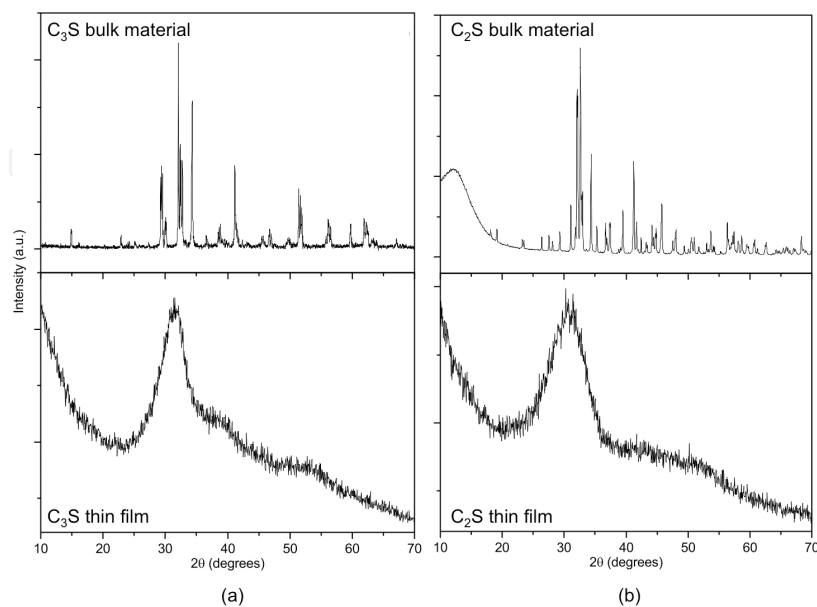
Figure 1. (a) C_3S powder (top) and grazing incident angle (bottom) XRD from the bulk and thin film samples, respectively. (b) C_2S powder (top) and grazing incident angle (bottom) XRD from the bulk and thin film samples, respectively.
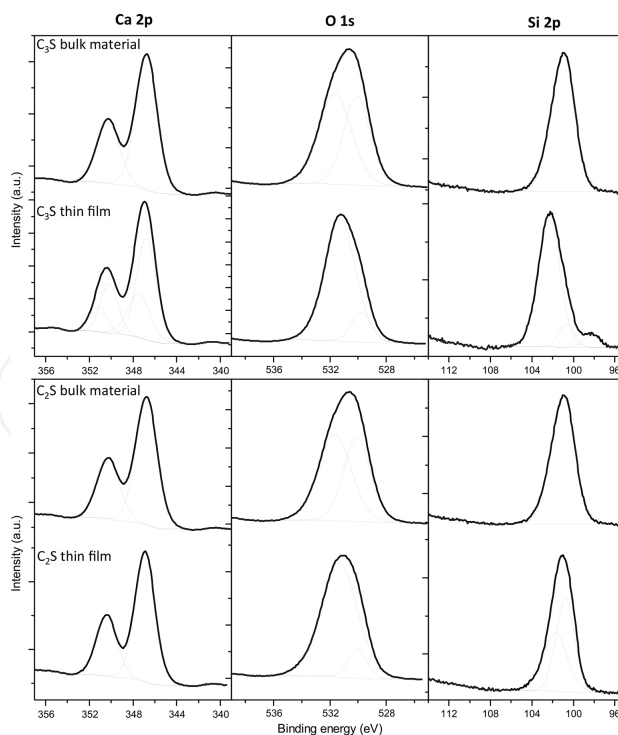
Figure 2. Top: XPS spectra of the C_3S (top) and C_2S (bottom) bulk material and thin film. Thick lines are the spectra collected, while the thin lines are the background and the result of peak fitting.

On the other hand, a comparison between XPS patterns from bulk material and the thin film shows that the elements are present in the same elemental coordination state. Some changes are noticed though, as an additional calcium peak at 351.1 eV, which can be related to pre-hydration on the surface due to the contact with the atmosphere. The same behavior was observed in previous researches [3, 4]. This is confirmed by the silicon peak, which presents a split into two peaks at 102.4 and 100.6 eV. This shift to higher BE is related to pre-hydration and the formation of C-S-H [18]. At the same time, there is the presence of a peak related to the metallic silicon from the thin film (98.2 eV), which is associated with the substrate and is probably due to the porosity of the layer, despite its thickness (**Figure 2**); hence, reaction with the substrate cannot be totally discarded [19]. Changes in the oxygen peak positions are also related to this pre-hydration effect.

Likewise, XPS results assure that the evaporated C_2S chemical material is very similar to the bulk material, with the peaks located at the same BE and with similar FWHM values (**Figure 2**), and the appearance of a new silicon peak, together with the slight shifts in the oxygen peaks energy, can also be attributed to the substrate as well as to pre-hydration. On the other hand, magnesium (a minor component in the original bulk material) is also detected in the thin film spectrum.

2.2. Calcium aluminates

C_3A films exhibit better-defined GIXRD peaks (**Figure 3a**), less noise and higher intensity than the silicate samples. This is due to the larger sample used for the test, which provides larger area for analysis, since the detector aperture can be larger, allowing more signal to be collected. In this case, the film produced from the evaporation of C_3A was formed by other phases (including calcite, lime and portlandite; **Figure 4a**), but no phases with aluminum are identified.

The evaporated C_4AF has a similar behavior to C_3A. In this case, the GIXRD spectrum is not conclusive as it is extremely noisy and indicates the formation of amorphous materials (**Figure 3b**). For the bulk material, the peaks correspond to Brownmillerite, or C_4AF, except for one peak at 18.11°, which may be related to the presence of Fe_3O_4, which cannot be discarded, as discussed later in the XPS analysis.

Diffraction data are confirmed by the XPS analyses, which show that the calcium is deposited in similar chemical state as in the bulk material (shifts of 0.2–0.3 eV), but the aluminum peak does not appear in the thin film spectrum, meaning that it did not recondense on the substrate (**Figure 4**).

C_4AF bulk and thin film present Fe 2p peaks with two components, indicating the presence of two compounds (**Table 3**, **Figure 4**). The BE themselves are not conclusive of what compounds are present, as the observed BEs are similar to the ones of Fe_2O_3, Fe_3O_4 and FeO. While the Fe 2p components at lower BE present negligible changes from the bulk to the thin film, the second component at higher energies presents significant changes (about +0.7 eV); this indicates strong bonding changes in iron after the evaporation. Since differences in the O 1s BE are observed as well by shifts of +0.4 and +0.8 eV, differences between this two samples are clear. Finally, Ca

2p peaks shift to higher energies by +0.7 eV, indicating again differences in the thin film material.
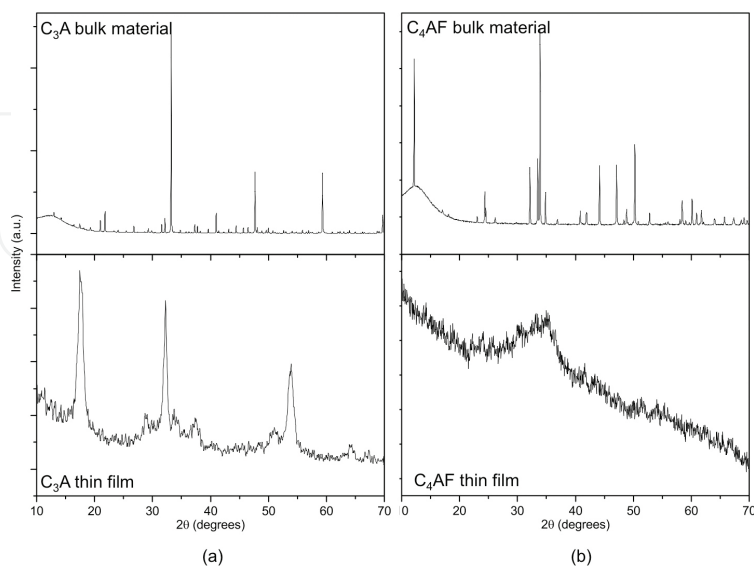

Figure 3. (a) C_3A powder (top) and grazing incident angle (bottom) XRD from the bulk and thin lm samples, respectively. (b) C_4AF powder (top) and grazing incident angle (bottom) XRD from the bulk and thin lm samples, respectively.
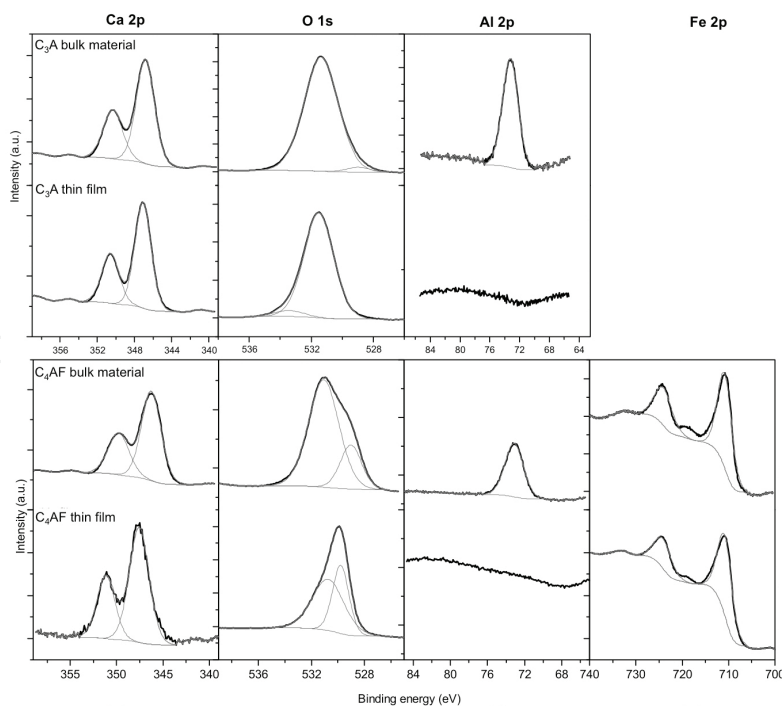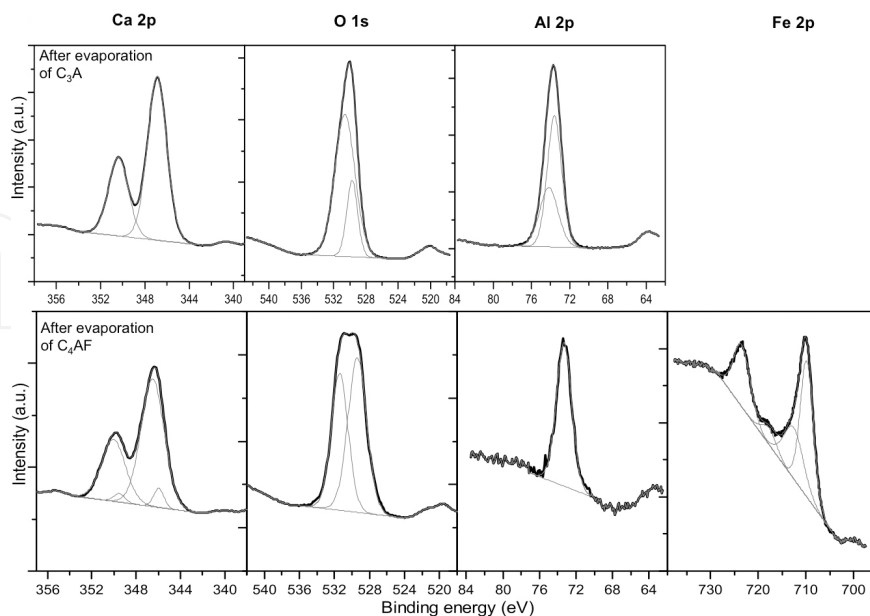

Figure 4. XPS spectra of the C_3A (top) and C_4AF (bottom), for their respective bulk material and thin film. Thick lines are the spectra collected, while the thin lines are the background and the result of peak fitting. XPS spectra for Ca 2p, O 1s, Al 2p and Fe 2p (for C_4AF only) are shown.

Analysis of the material left in the crucible after the evaporation of C_3A shows the presence of tricalcium aluminate and mayenite ($Ca_{12}Al_{14}O_{33}$ or $C_{12}A_7$; **Figure 5a**). $C_{12}A_7$ is formed from the phase that liquefied during the evaporation, indicating at least partially incongruent evaporation of C_3A, yielding to an evaporate/condensate that is substantially richer in Ca (note that the Ca/Al ratio of mayenite is 0.86, about 3.5 times lower than that of C_3A, and hence, the Ca enrichment of the evaporate can be inferred). The presence of portlandite and calcite in the thin films can therefore be interpreted as partial hydration and carbonation of a Ca-rich phase upon atmospheric exposure (although limited) of the thin films.
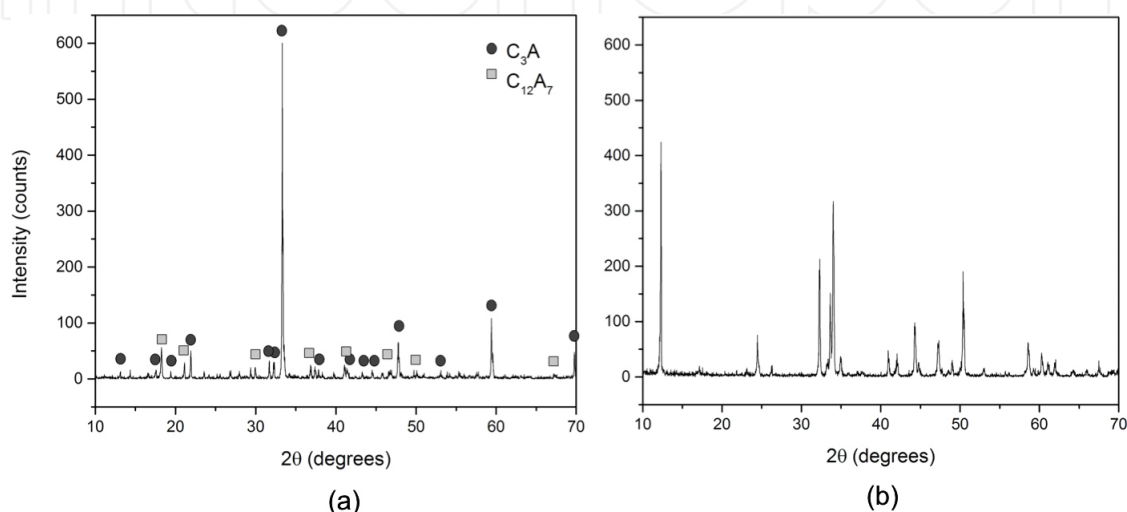
Figure 5. XRD of the residue left in the crucible after the evaporation of (a) C_3A and (b) C_4AF.

Figure 6. XPS spectra of the material left in the crucible after evaporation of C_3A (top) and C_4AF (bottom). Thick lines are the spectra collected, while the thin lines are the background and the result of peak fitting.

The absence of Al in the XPS spectra (**Figure 6**) could be due to some reaction scavenging from the silicon substrate, leading to aluminosilicates, similarly to what has been observed by Toda et al. [19] during production of $C_{12}A_7$ thin films. However, XPS data do not show any evidence of silicon, while reaction at deeper regions cannot be excluded, as on XPS the X-rays only penetrate a few nanometers on the surface.

Before completion of C_3A evaporation, a liquid phase formed while, probably, the bulk material was being converted into a mix of solid CaO and liquid calcium aluminate, with higher aluminum content than the initial C_3A. Possibly, only the solid phase evaporated and became the precursor of the generated thin film, since no aluminum is observed there.

The BE of the calcium peaks does not present relevant shifts from those in the bulk material. However, oxygen and aluminum peaks in the melt residue in the crucible present significant changes in both BE and FWHM (**Table 3**, **Figure 6**), which indicates a different coordination state.

Electron beam bombardment of C_4AF led, as in the case of C_3A, to the formation of a liquid phase, with a higher concentration of aluminum than in the bulk material. The phase diagram of $CaO-Fe_2O_3-Al_2O_3$ [20] shows that, when there is an incomplete fusion, the equilibrium is reached with a $Ca_2(Al,Fe^{+3})_2O_5$ phase with higher content of Fe (solid) and one liquid phase mix of $CaO.Al_2O_3$, without Fe. Analogous formation happens in the C_3A at up to 1542°C, when the equilibrium is reached for CaO solid + liquid (~40%wt of Al_2O_3 + CaO).

XRD patterns of the bulk material (**Figure 3a**) and the residue left in the crucible after the evaporation (**Figure 5a**) are remarkably similar. The main component in both materials is brownmillerite ($Ca_2(Al,Fe^{+3})_2O_5$); however, the presence of Fe_3O_4 or $Ca_2Al_{1.38}Fe_{0.62}O_5$ cannot be discarded.

In fact, Taylor [20] stated that "iron-rich mixes tend to lose oxygen when heated in air above 1200–1300°C, with consequent replacement of hematite by magnetite (Fe_3O_4)," which is in accordance with the observations here, even though it was not possible to verify the temperature in the crucible during the evaporation.

Likewise in the C_3A sample, during the evaporation of C_4AF, the material in the crucible melted and there were eruptions, as well as there was no aluminum in the film. That means the residue left in the crucible has to be richer in aluminum. Again, as observed for the C_3A sample, reaction with the substrate at deeper regions, as observed by Toda et al. [19], cannot be discarded. However, no XPS signal of silicon can be detected, suggesting that such a reaction does not occur.

In the same way, the XPS analyses for the material left in the crucible after the evaporation of the C_4AF (**Figure 5b**) present a strong difference when compared to the initial bulk material: Fe 2p peak presents only one component at 709.8 eV (Fe 2p3/2) and 723.0 eV (Fe 2p1/2), meaning important changes happened in the chemical/electronic state of this element. O 1s presents BE shifts of +0.3 eV and Ca 2p of -0.5 eV, while BE of Al 2p is similar to the starting material (**Table 3**).

The XPS 2p spectra of Fe, as other transition metals, present complex lineshapes due to the electrons exchange interaction effects, as well as electron correlation effects [21]. Normally, Fe 2p peaks are broad, asymmetric and may contain satellites, which are observed here as well.

On the other hand, for iron oxides, the O 1s BE is expected to increase with a decrease in the oxidation number of the cation of the same metal; it is observed here an increase in O 1s BE by +0.3 eV from the bulk to the material left in the crucible. At the same time, Graat and Somers [22] describe an increase in BE for increase in oxidation state of iron; here, this is very much evident as with the existence of only one iron component, which still presents a BE lower by -0.4 eV than the Fe 2p peak with the lowest BE in the bulk material (709.8 vs 710.2 eV), suggesting a decreasing in the oxidation state for the material left in the crucible (**Table 3**).

This may explain the possible existence of $Ca_2Al_{1.38}Fe_{0.62}O_5$, besides the brownmillerite, in the material in the crucible, as XRD could suggest. This compound was also observed by Vázquez-Acosta et al. [23].

The phase diagram for the C_4AF partial fusion relates to a solid phase C_2F ($2CaO.Fe_2O_3$) and a liquid with composition similar to the $Ca_2(Al_xFe_{1-x})O_5$, in direction to phases with higher aluminum concentration than the C_4AF itself. As underlined by Taylor [20] "for bulk compositions in the $Ca_2(Al_xFe_{1-x})O_5$ series, the liquid is of higher Al/Fe ratio than the ferrite phase with which it is in equilibrium."

3. Hydration of calcium silicate thin films

Calcium silicates' hydration happens over a dissolution-precipitation process that may occur through the formation of etch pits, where the calcium silicate hydrate (C-S-H) preferentially precipitates, together with calcium hydroxide (portlandite or CH), the two hydration products. C-S-H is the main product formed by the hydration of the calcium silicates and responsible for the strength of the cement paste. It is mostly amorphous, and the dashes indicate a disordered structure. Its particle density was found by Gauffinet et al. [18] to be in the order of $2500 \, kg/m^3$.

At the molecular level, C-S-H has a structure similar to the tobermorite ($Ca_5Si_6O_{16}(OH)_2 \cdot 8H_2O$) and jennite ($Ca_9Si_6O_{18}(OH)_6 \cdot 8H_2O$), rare minerals found in nature. Most of the models predicting the C-S-H nanostructure involve elements of jennite-like or even tobermorite-jennite structures [26].

After running the initial pattern presented previously (**Figures 2** and **3**), C_3S and C_2S dry thin film samples were hydrated separately in a reaction chamber that was located in the same vacuum line as the XPS, hence avoiding any hydration and/or carbonation from the contact with the atmosphere. Saturated water vapor with argon as a carrier was inserted at 20 mL/min. Prior to hydration, the system was purged for 5 min to avoid any contamination.

XPS analyses of the hydrated 110-nm-thick C_3S thin film are presented in detail in Ref. [3]. Results show, after 3 h of exposure to water vapor, a shift in the Si 2p peak of about 0.7 eV (from

101.9 to 102.6 eV) (**Table 4**), while the literature reports lower BE for this peak (100.57 eV in fresh C_3S, [6]). This indicates a progressive disordering of the silicate structure, which denotes the C-S-H formation.

Time	Peak positon (eV)			Ca/Si ratio
(mins)	Si 2p	δCa 2p-Si 2p	Ca 2p 3/2	Ca 2p/Si 2p
0	101.9 (2.5)	245.2	346.8 (2.7)	3.4
2	101.9 (2.4)	245.3	347.0 (2.7)	3.4
7	102.2 (2.4)	245.1	347.1 (2.6)	3.4
12	102.4 (2.5)	245.0	347.3 (2.6)	3.4
17	102.4 (2.5)	244.9	347.3 (2.6)	3.4
27	102.6 (2.6)	245.0	347.4 (2.5)	3.8
42	102.5 (2.5)	244.9	347.4 (2.5)	3.6
62	102.6 (2.5)	244.9	347.4 (2.5)	3.6
122	102.6 (2.5)	244.6	347.2 (2.5)	3.5
182	102.6 (2.5)	244.6	347.2 (2.5)	3.6

Table 4. Evolution of binding energies and peak width (FWHM) of Si and Ca, Ca-Si peak distance and Ca/Si ratio during vapor hydration of C_3S.

The measurement of the energy separation δCa 2p-Si 2p between the Ca 2p 3/2 and Si 2p peaks minimizes errors due to the charge correction and provides reliable information on chemical changes [8, 24]: Shifts on Si peaks to higher BE due to the progressive hydration of C_3S lead to reduction in the distance between the peaks of calcium and silicon, as there is a polymerization of the isolated silicate tetrahedra upon formation of C-S-H, and/or carbonation [9]. However, the formation of calcium carbonate is unlikely to occur here due to the nature of the experiments. Initial δCa 2p-Si 2p values found here (245.3 eV) are lower than those from the literature [6, 24, 25]; however, the decrease in the Ca-Si distance after 3 h of hydration of C_3S (δCa 2p 3/2 - Si 2p = 0.6) is identical to that found by [24] after 4 h.

In the same way, the molar Ca/Si ratio of the newly formed hydrates Ca/Si ratio remains the same, as the expected isochemical conditions of the experiment. The excess Ca content (Ca/Si of about 3.5 vs. 3.0 of stoichiometric tricalcium silicate, **Table 4**) during the early hydration can be related to fast partial hydration and carbonation of the upper few nanometers of the sample during manipulation under atmospheric conditions prior to the experiments.

However, peak deconvolution of the Ca 2p 1/2 peaks shows contributions from carbonates and silicates: Calcium silicates have Ca 2p BE slightly higher than those of calcium carbonates. Considering only the calcium related to silicates in this equation, the Ca/Si ratio drops from the initial 1.6 to 0.5, as hydration progresses. Such low values indicate a progressive polymerization of silicate tetrahedra and subsequent increase in C-S-H chain

length, equivalent to an increase in SiO_2 content [9, 26]. These results agree with Taylor [26], who suggests that the first precipitate is a jennite-like material, with a Ca/Si ratio of about 1.5, evolving to a tobermorite-like material as the hydration progresses. Detailed information on the tobermorite and jennite structure can be found elsewhere [20, 26].

The same experimental procedure was used for the hydration of a 200-nm-thick C_2S thin film (presented in detail in [4]), which, with exposure to water vapor, shows a similar drift of the main Si 2p peak, from 101.2 to 102.6 eV, denoting the disordering of the silicate structure related to progressive C-S-H formation (**Table 5**). This shift is accompanied by a peak broadening at higher ages, forming an additional peak at around 100.2 range, same as described by Black et al. [6], where a Si 2p 3/2 BE of 100.8 eV is observed for the fresh C_2S and followed by two peaks at 102.44 and 100.51 eV, which are seen for the aged sample. The peak at lower energies is related to unaltered β-C_2S, while the peak at higher binding energy is assigned to a calcium-depleted C-S-H phase.

Age (min)	Binding energy (eV) and (FWHM)				Ca-Si distance (eV)	NBO-BO distance (eV)
	Si 2p	Ca 2p 3/2	O 1s NBO	O 1s BO	δCa 2p-Si 2p	δNBO-BO
0	101.2 (2.6)	347.0 (2.1)	530.1 (1.5)	531.4 (3.0)	245.8	1.3
2	101.4 (2.6)	347.1 (2.1)	530.3 (1.4)	531.5 (3.1)	245.7	1.2
7	101.7 (2.7)	347.3 (2.6)	530.4 (1.5)	531.7 (3.0)	245.7	1.3
12	101.6 (2.8)	347.3 (2.2)	530.3 (1.3)	531.7 (3.1)	245.7	1.3
17	101.8 (2.9)	347.5 (2.1)	530.3 (1.2)	531.9 (3.0)	245.8	1.5
27	101.9 (2.8)	347.4 (2.1)	530.3 (1.5)	531.9 (2.8)	245.5	1.5
42	102.0 (2.9)	347.4 (2.2)	530.2 (1.8)	531.9 (2.9)	245.5	1.7
62	100.2 (1.2) 102.0 (2.9)	347.5 (2.2)	530.4 (2.0)	532.1 (2.8)	245.5	1.7
122	100.1 (1.2) 102.1 (2.8)	347.5 (2.2)	530.2 (2.0)	532.1 (2.8)	245.4	1.8
182	100.2 (1.3) 102.4 (2.9)	347.7 (2.3)	530.4 (1.9)	532.2 (2.8)	245.3	1.9
272	100.2 (1.7) 102.5 (2.8)	347.6 (2.3)	530.2 (1.8)	532.2 (2.8)	245.1	1.9
632	100.4 (1.4) 102.6 (2.8)	347.7 (2.2)	530.4 (2.0)	532.3 (2.8)	245.1	1.9

Table 5. Evolution of binding energies of Si, Ca and O (peak width, FWHM), Ca-Si peak distance and NBO-BO peak distance during vapor hydration of C_2S.

The Ca BE, on the other hand, shows a small progressive shift (0.7 eV) when hydration goes on. The Ca 2p3/2 peak is centered at around 347.0 eV (**Table 5**) for fresh C_2S, a value slightly lower than the one previously reported by Black et al. [6] (347.23 eV).

The initial energy separation between Ca 2p 3/2 and Si 2p peaks found in this work (245.8 eV) is fairly lower than those reported by Black et al. [6], (246.72 eV). The progressive hydration of C_2S results in shifting of the Si 2p peak to higher BE, therefore reducing the δCa 2p-Si 2p, due to the polymerization of the isolated silicate tetrahedra upon formation of C-S-H.

The molar Ca/Si ratio of the newly formed hydrates in C_2S thin film starts with a lower value than expected from the bulk material (initial Ca/Si of about 1.6 vs. 2.0 of stoichiometric dicalcium silicate), indicating a partial hydration of the upper few nanometers of the sample during manipulation under atmospheric conditions, and decreases over time, reaching Ca/Si = 1.0. The same values are described by Regourd et al. [24], who found this value after 4 h of hydration. While small contributions from portandite and/or unhydrated C_2S cannot be excluded, such low Ca/Si values clearly evidence the formation of C-S-H. Here, different peaks related to the contributions from carbonates and silicates are not observed.

In this sample, it was possible to study the O 1s spectrum, which provides important information on the structure of minerals and glasses but is complex to be assessed. O 1s can be present in different components, which have different BE: non-bridging oxygen (530–530.5 eV), bridging oxygen (531.5–532.7 eV), hydroxide species (533–533.5 eV), bound water (534 eV) and portlandite at calcium-rich samples (531.6 eV), while amorphous silica does not add any extra component [27].

Changes in the peaks separation between bridging and non-bridging oxygen atoms (δNBO-BO) are related to silicon polymerization: Peak distance grows with the falling of the Ca/Si ratio that happens together with hydration by water vapor, since the contribution from non-bridging oxygen decreases as the hydration progresses (the number of Ca-O-Si units decreases and Si-O-Si units increases), as observed in **Table 5**.

4. Final remarks

The fact that the chemical and mineralogical composition of the calcium silicate thin films is in accordance with the respective bulk materials proves that the electron beam evaporation is a useful and powerful way for synthesizing thin films of calcium silicates. However, not the same was observed for the calcium aluminate phases: The electron beam evaporation conditions used in this work are not suitable for producing thin films of these materials. Chemical and mineralogical analysis of the residue left in the crucible after the evaporation shows that the aluminum present on these phases does not evaporate, and for this reason, there is no signal of this element in the thin films. Aluminum reacts abnormally when submitted to the extreme conditions during the sample preparation.

This behavior is clearly observed with the GIXRD and XPS data. Even as the electron beam evaporation fails to provide the expected results for the evaporation of phases containing

aluminum, other standard techniques for producing ceramic thin films can be applied. Presumably, sputtering may allow synthesizing thin films of these phases as in this technique the sample is not heated. Instead, atoms are ejected through the bombardment of the target material by energetic particles.

The difficulty on using sputtering techniques arises from the fact that it is challenging to have suitable targets as it demands unusual preparation and generally companies that manufacture them refuse to produce targets with special specifications. In this case, additional manufacturing effort is needed for producing targets so that this technique can be applied for the synthesis of thin films of clinker phases.

This type of sample has been proven to be useful in attaining information related to dissolution, hydration and carbonation in ways never before explored. Research using thin films of clinker phases for hydration analysis is found elsewhere [3, 4].

XPS provides information on the upper few nanometers of the sample only, being suitable for thin films studies, offering accurate chemical composition and coordination state data. Regarding the XPS data for all the C_3S and β-C_2S samples, the peak positions, peak distances and peak widths are typically equivalent to the bulk material, proving that they have the same chemical composition. However, pre-hydration is observed due to the contact of the sample with the atmosphere.

Hydration of C_3S presented shifts on Si 2p peak to higher BE, related to silicon polymerization by the formation of C-S-H. The δCa 2p-Si 2p distance decreased with time, indicating that the kinetics of early C-S-H formation is not significantly altered when vapor is used instead of liquid water.

The molar Ca/Si ratio in both C_2S and (from carbonate contribution) C_3S decreases as the hydration proceeds, due to the progressive polymerization with an increase in chain length of the silicate hydrates formed. Initial Ca/Si values in C_3S correspond to a jennite-like material and evolve to a tobermorite-like component after 3 h of exposure to water.

Some possible pre-hydration is observed in both calcium carbonates, by the contact with the atmosphere during the sample manipulation or due to the preferential deposition of the silicon on the sample's surface after the evaporation. Besides that, the peak positions of the bulk material are maintained and so the chemical state.

The C_2S samples provided clearly distinguished O 1s spectra, allowing to identify the δNBO-BO peak separation, which increases with the silicon polymerization, describing the C-S-H formation.

Acknowledgements

of Science and Innovation. The authors also thank Diogo Topolski for the help with the XRD analysis.

Author details

Vanessa Rheinheimer[1*] and Ignasi Casanova[2]

*Address all correspondence to: vanessa.rhe@gmail.com

1 Berkeley Education Alliance for Research in Singapore—BEARS, Create Way, Singapore

2 Department of Construction Engineering and Center for Research in Nanoengineering, Polytechnic University of Catalonia—Barcelona Tech., Barcelona, Spain

References

[1] K. L. Scrivener and A. Nonat. Hydration of cementitious materials, present and future. Cem. Conc. Res. 2011;41(7):651–665.

[2] E. Dubina, L. Black, J. Sieber, and R. Plank. Interactions of water vapour with unhydrous cement minerals. Adv. Appl. Ceram. 2010;109:260–268.

[3] V. Rheinheimer and I. Casanova. Hydration of C3S thin films. Cem. Concr. Res. 2012;42:593–597.

[4] V. Rheinheimer and I. Casanova. An X-ray photoelectron spectroscopy study of the hydration of C2S thin films. Cem. Concr. Res. 2014;60:83–90.

[5] L. Black, A. Stumm, K. Garbev, P. Stemmermann, K. R. Hallam, and G. C. Allen. X-ray photoelectron spectroscopy of the cement clinker phases tricalcium silicate and β-dicalcium silicate. Cem.Conc.Res. 2003;33(10):1561–1565.

[6] L. Black, K. Garbev, P. Stemmermann, K. R. Hallam, and G. C. Allen. Characterisation of crystalline C-S-H phases by X-ray photoelectron spectroscopy. Cem. Concr. Res. 2003;33(6):899–911.

[7] L. Black, K. Garbev, and I. Gee. Surface carbonation of synthetic C-S-H samples: A comparison between fresh and aged C-S-H using X-ray photoelectron spectroscopy. Cem. Concr. Res. 2008;38(6):745–750.

[8] L. Black, K. Garbev, G. Beuchle, P. Stemmermann, and D. Schild. X-ray photoelectron spectroscopic investigation of nanocrystalline calcium silicate hydrates synthesised by reactive milling. Cem. Concr. Res. 2006;36(6):1023–1031.

[9]   M. Yousuf, A. Mollah, T. R. Hess, Y.-N. Tsai, and D. L. Cocke. An FTIR and XPS investigations of the effects of carbonation on the solidification/stabilization of cement based systems-Portland type V with zinc. Cem. Concr. Res. 1993;23(4):773–384.

[10] L. Dubina, E. Sieber, R. Plank, and J. Black. Effects of pre-hydration on hydraulic properties of Portland cement and synthetic clinker phases. Cem. Conc. Sci. 2008; 64:49–67.

[11] L. Nicoleau, E. Schreiner, and A. Nonat. Ion-specific effects influencing the dissolution of tricalcium silicate. Cem. Conc. Res. 2014;59:118–138.

[12] P. Dutta. Grazing incidence X-ray diffraction. Curr. Sci. 2000;78(12):1478–1483.

[13] M. Bouroushian. Characterization of thin films by low incidence X-ray diffraction. Cryst. Struct. Theory Appl. 2012;1(3):35–39.

[14] S.-L. Chang. Thin-film characterization by grazing incidence X-ray diffraction and multiple beam interference. J. Phys. Chem. Solids. 2011;62(9–10):1765–1775.

[15] V. R. Mastelaro, C. R. Foschini, and J. A. Varela. Grazing incidence X-ray diffraction and atomic force microscopy analysis of $BaBi_2Ta_2O_9$ thin films. Thin Solid Films. 2002;415(1–2):57–63.

[16] C.-H. Ma, J.-H. Huang, and H. Chen. Residual stress measurement in textured thin film by grazing-incidence X-ray diffraction. Thin Solid Films. 2002;418(2): 73–78.

[17] R. Thomas, N. K. Karan, P. Ehrhart, R. Waser, and R. S. Katiyar. Dysprosium scandate thin films prepared by metal organic chemical vapor deposition on Pt/TiOx/SiO2/Si substrates for MIM capacitor applications. ECS Transactions. 2007;11(4):529–540.

[18] S. Gaufinet, E. Finot, and A. Nonat. Experimental study and simulation of C-S-H nucleation and growth. Mater. Struct. 1997;38:435–442.

[19] Y. Toda, M. Miyakawa, K. Hayashi, T. Kamiya, M. Hirano, and H. Hosono. Thin film fabrication of nano-porous $12CaO_7Al_2O_3$ crystal and its conversion into transparent conductive films by light illumination. Thin Solid Films. 2003;445(2):309–312.

[20] H. F. W. Taylor. Cement Chemistry. Thomas Telford Publishing ed.; London: 1997.

[21] E. Paparazzo. On the quantitative XPS analysis of Fe_2O_3 and $Fe_{1-x}O$ oxides. J. Electron Spectros. Relat. Phenomena. 2006;154(1–2):38–40.

[22] P. C. J. Graat and M. A. J. Somers. Simultaneous determination of composition and thickness of thin iron-oxide films from XPS Fe 2p spectra. 1996;36–40.

[23] F. Vázquez-Acosta, L. M. Torres-Martínez, W. López-González, and J. Ibarra-Rodrí-guez. Influence of iron content on the color of the C3A–Fe2O3 system synthesized under different conditions of temperature, atmosphere and cooling. Ceram. Int. 2012;38(4):3261–3272.

[24] M. Regourd, J. H. Thomassin, P. Baillif, and J. C. Touray. Study of the early hydration of Ca3SiO5 by X-ray photoelectron spectrometry. Cem. Concr. Res. 1980;10(2):223–230.

[25] S. Long, C. Liu, and Y. Wu. ESCA study on the early C3S hydration in NaOH solution and pure water. Cem. Concr. Res. 1998;28(2):245–249.

[26] H. F. W. Taylor. Proposed structure for calcium silicate hydrate gel. J. Am. Ceram. Soc. 1986;69(6):464–467.

[27] M. Regourd, C. Defosse, S. A. Jefferis, and J. Bensted. Microanalytical studies (X-ray photoelectron spectrometry) of surface hydration reactions of cement compounds [and discussion]. Philos. Trans. R. Soc. London. Ser. A, Math. Phys. Sci.. 1983;310(1511): 85–92.